

Experimental and numerical study on innovative seismic T-Resisting Frame (TRF)

Payam Ashtari¹, Helia Barzegar Sedigh^{*2} and Farzaneh Hamed²

¹Department of Civil Engineering, University of Zanjan, Zanjan, 45371-38791, Iran

²Department of Civil Engineering, Imam Khomeini International University, Qazvin, 34149-16818, Iran

(Received September 16, 2015, Revised May 12, 2016, Accepted June 30, 2016)

Abstract. In common structural systems, there are some limitations to provide adequate lateral stiffness, high ductility, and architectural openings simultaneously. Consequently, the concept of T-Resisting Frame (TRF) has been introduced to improve the performance of structures. In this study, Configuration of TRF is a Vertical I-shaped Plate Girder (V.P.G) which is placed in the middle of the span and connected to side columns by two Horizontal Plate Girders (H.P.Gs) at each story level. System performance is improved by utilizing rigid connections in link beams (H.P.Gs). Plastic deformation leads to tension field action in H.P.Gs and causes energy dissipation in TRF; therefore, V.P.G. High plastic deformation in web of TRF's members affects the ductility of system. Moreover, in order to prevent shear buckling in web of TRF's members and improve overall performance of the system, appropriate criteria for placement of web stiffeners are presented in this study. In addition, an experimental study is conducted by applying cyclic loading and using finite element models. As a result, hysteresis curves indicate adequate lateral stiffness, stable hysteretic behavior, and high ductility factor of 6.73.

Keywords: T-Resisting Frame; experimental study; finite element; link beams; shear yielding; ductility factor

1. Introduction

Application of seismic design codes is essential to prevent structural failure under severe earthquakes and ensure lateral stability. Therefore, it is required to propose lateral resistant systems by emphasizing providing sufficient ductility, strength, and lateral stiffness to dissipate earthquake-induced energy. Since an increase in stiffness results in a decrease in ductility, it is desirable to devise a structural system which provides these properties in an optimum level without excessive costs.

TRF consists of Vertical Plate Girder (V.P.G) with high depth of web, which is located at the middle of span and jointed to side columns by two Horizontal Plate Girders (H.P.Gs). Using the entire capacity of H.P.Gs' web with respect to tension field theory, rigid connections of link beams (H.P.Gs), and even rigid base connection of TRF's vertical members may improve the performance. Firstly, the flexural yield of TRF members, connection method, and the number of

*Corresponding author, MSc., E-mail: helia.barzegarsedigh@yahoo.com

V.P.Gs has been studied (Ashtari and Bandehzadeh 2009, Ashtari and Abbasi 2010, Bandehzadeh and Ashtari 2014). This lateral resistant system was also checked by performing Endurance Time method (ET) as a dynamic structural analysis (Riahi and Estekanchi 2010) which confirms the suitable flexural yield of TRF's members with different span lengths and alternate heights (Gorzin 2011). In comparison to Eccentrically Braced Frames (EBFs), more ductility and better performance was obtained due to initial shear yielding specially in H.P.Gs caused by decreasing their length (Ashtari *et al.* 2012). The seismic characteristics of TRF against shear and flexural yielding of H.P.Gs were investigated by Barzegar Sedigh (2013), and H.P.Gs' shear yielding achieved as a proof of TRF's better performance. Collapse assessment of structural systems using hysteretic models has been emphasized by many researchers in order to modify the Ibarra-Krawinkler deterioration model (Chao and Goel 2005, Lignose and Krawinkler 2008). In this regard, hysteresis curve of members with shear yielding is investigated in this paper. An appropriate performance of system was observed primarily by shear yielding of H.P.Gs and then V.P.G. According to related literatures and basis assumption of seismic design, H.P.Gs is approximated to link beam in EBF, and V.P.G performs as a stiffened shear wall without elastic buckling. Section properties of the V.P.G and H.P.Gs have a major effect on the ductility and energy dissipation of the TRF systems. In this paper, actual behavior, ductility factor, and fracture modes are assessed in TRF specimen by applying cyclic loading. Shear yielding specially in H.P.Gs is studied by eight finite element models for verifying the numerical results from the test and also developing the numerical studies.

2. Introducing TRF and its concepts

The new TRF system is an I-shaped steel beam (V.P.G) which is vertically placed within the span, connected with two other Horizontal Plate Girders (H.P.Gs) as link beams, to the side columns at each story level (Fig. 1). Improvement of the system is provided by the use of rigid connections in H.P.Gs. TRF is introduced based on its configuration to have a shear or flexural yielding of horizontal link beams and secondly, the yield of stiff vertical beam mounted in middle of the frame span and causes an increase in the capacity of plastic chord rotation together with lateral stiffness (Barzegar Sedigh 2013). Assumptions of fixed or simple base joint of side columns are compared to provide appropriate seismic characteristics (Barzegar Sedigh 2013). This

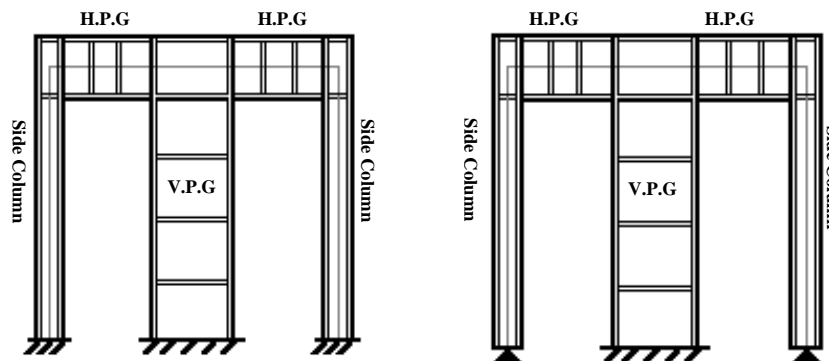


Fig. 1 Configurations of TRF with side columns: (Left) fixed and (Right) simple base joint

will fulfill architectural considerations such as locating openings while considering seismic regulations (Bandehzadeh and Ashtari 2014).

Load distribution in T members would result in better performance of system by controlling the axial force of side columns and also by creating more resisting moment in base due to V.P.G. This results in an economical joint design (Bandehzadeh and Ashtari 2014).

Novelty of TRF needs more attention to design parameters such as width to thickness ratio. As it is possible for V.G.P's web to be compact or even non-compact, the stability and stiffness can be provided by web stiffeners. In comparison to EBF system, compression force and shear buckling of web in plastic zone are controlled with an optimal design by applying simple base joint in TRF side columns. In addition, considering flange compaction requirements in V.P.G and placing horizontal web stiffeners in appropriate place, cause the elastic, global and local buckling to be precluded. In this case, stable and growing hysteresis curve without loss of lateral resistance and stiffness, are derived. It can be inferred that TRF with yield of three ductile members and lateral stability presents better seismic lateral behavior.

3. Seismic provisions and parameters

3.1 Design of transverse stiffeners

Web stiffeners of H.P.Gs are designed for purposes such as increasing stiffness which leads to primary and progressive yield, provide shear resistance, control local buckling, and shear deformations. Primary distance (a) assumption is used as EBF's link beam with limited link rotation angle as 0.02 rad by Eq. (1) (d : web height, t_w : web thickness). For more conservative design, minimum distance can be reduced to values given by Eq. (2) in AISC341-10 (2010).

$$a = 50 \cdot t_w - \frac{d}{5} \quad (1)$$

$$a = 30 \cdot t_w - \frac{d}{5} \quad (2)$$

V.P.G's web stiffeners are designed in order to maintain general and local stability with respect to the fact that V.P.G as a ductile member of TRF is not designed to resist plastic shear capacity of H.P.Gs.

Here, the distance of web stiffeners is proposed as an average of upper limit of stiffeners' distance of H.P.Gs and transverse stiffeners distance which are used to develop the available web shear strength (shown by a_{oi}). This proportion is expressed by Eq. (3).

$$a = \frac{(50 \cdot t_w - \frac{d}{5}) + a_{oi}}{2} \quad (3)$$

3.2 Yielding parameters and chord rotation

H.P.Gs rotation capacity with shear yielding is similar to link beams in EBFs in which link beams' length is less than $\frac{1.6M_P}{V_P}$ (M_P : Plastic Moment strength, V_P : Plastic Shear strength).

Equivalent stiffness calculated by combination of shear and flexural stiffness will cause further high chord rotation capacity in different performance levels by calculating yield chord capacity ($\theta_y = \gamma_y$) according to Eqs. (4)-(7) (F_y : Yield strength, A_w : Web area, Q_{CE} : Expected strength, K_s : Shear stiffness, K_b : Flexural stiffness, K_{eq} : Equivalent stiffness) (FEMA 356 (2000)).

$$V_P = 0.6F_y \cdot A_w \quad (4)$$

$$Q_{CE} = M_{CE} = \frac{V_P \cdot e}{2} \quad (5)$$

$$K_{eq} = \frac{K_s \cdot K_b}{K_s + K_b} \quad (6)$$

$$\theta_y = \gamma_y = \frac{V_P}{e \cdot K_{eq}} \quad (7)$$

In order to calculate chord rotation parameters of H.P.Gs, according to FEMA356 (Table 5.6) and FEMA 274, absolute rotation values of EEBs' link beams with shear yielding are modified by applying coefficient of $\frac{\gamma_y}{0.01}$.

V.P.G with high shear stiffness and greater depth than other TRF's members is similar to stiff steel shear wall plastic rotation. Therefore, plastic chord rotation will be calculated by Basler formula (Sabouri 2001). This is more than rotation capacity of column in Special Moment Resisting Frames (SMRF). Finally, P-M hinge is applied to side columns with respect to columns of SMRF according to FEMA356 (2000).

3.3 Ductility factor

The proportions of structure's maximum lateral displacement (Δ_{max}) to yield limit (Δ_y) known as μ , is determined by Eq. (8) (Hajnajafi and Tehranizadeh 2013).

$$\mu = \frac{\Delta_{max}}{\Delta_y} \quad (8)$$

3.4 Loading protocol

For primary estimation of system's behavior without applying seismic records, cyclic loading protocol can be used (Krawinkler 2009).

Moment frame's cyclic load protocol is chosen according to AISC-Seismic Provision2010 (Fig. 2). This protocol is considered due to ratio of lateral displacement (Δ) of load applying zone, to the height of the same elevation (H) using Eq. (9) according to AISC341-10 (2010).

$$\theta = \frac{\Delta}{H} \quad (9)$$

3.5 Shear deformation

Shear deformation (δ_v) in web panel is studied by translational and relative deformation of two

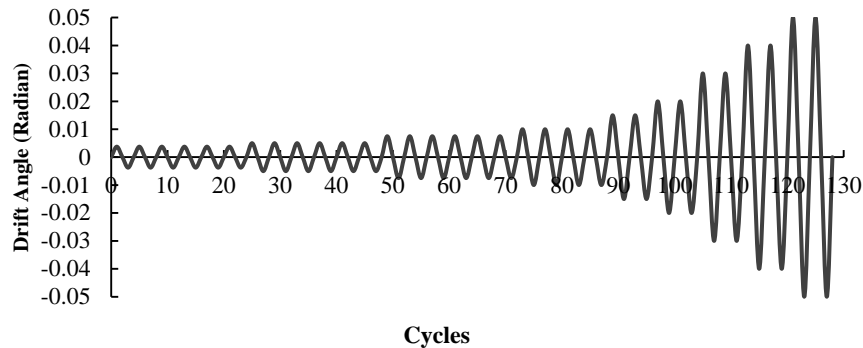


Fig. 2 Cyclic load protocol (AISC 341-10 2010)

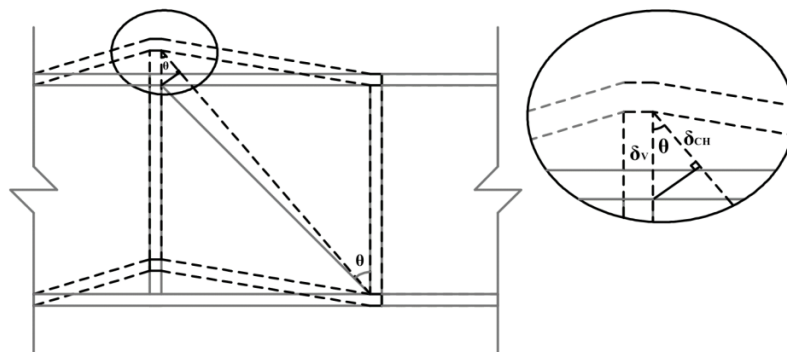


Fig. 3 A schematic view of shear deformation and chord rotation in web panel

points at two ends of it (δ_{Ch}), according to Eq. (10) (Fig. 3). This parameter is the most important data achieved by shear yielding of members.

$$\delta_v = \frac{\delta_{Ch}}{\cos \theta} \tag{10}$$

4. Modeling

4.1 Details of modeling and design

Experimental sample with 1:2 scale is derived from the top story of an ordinary five-story building (Farshchi *et al.* 2011). Surveys are done over half scale 3D structure, according to former studies (Ashtari *et al.* 2012) with 1.5 m story height, by applying Special Concentrically Braced Frames (SCBFs) in the 12 meters long direction and TRF in three spans located at sides and middle of the direction with 6.75 m length as shown in Fig. 4 (Locations of TRF system are shaded). Span length of TRF is selected equal to certain length which may lead to shear yielding of H.P.Gs, equal to $\frac{1}{5}$ of span in former studies. Static analysis parameters are applied according to ASCE-7-10 shown in Table 1. Effects of large deformations are considered.

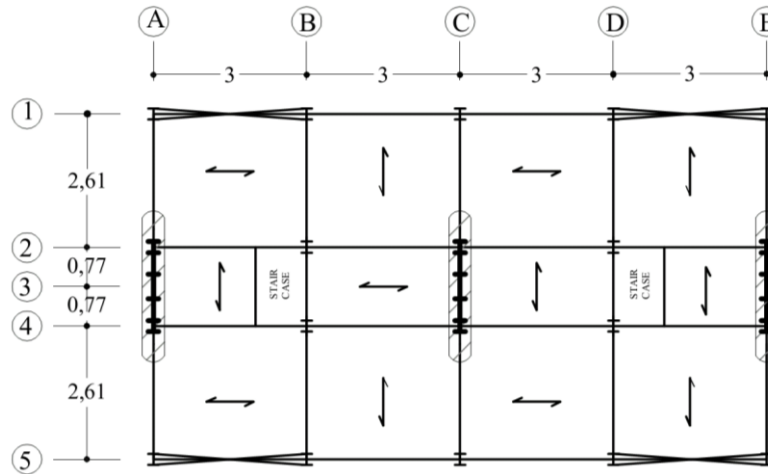


Fig. 4 1:2 scaled prototype building story plan

Table 1 Linear static analysis parameters for 5 story building of Fig. 4

Type of soil: <i>D</i> , Seismic Design Category: <i>D</i>	
$T_O=0.15$ s	$T_O=0.15$ s
$I=1, \rho=1, K=1, \Omega=2$	
$R_{WY}=8$	$R_{WX}=6$
$T_Y=0.33=0.0731(7.5)^{3/4}$	$T_X=0.22=0.0448(7.5)^{3/4}$
$C_d=5$	$C_d=4$
$S_1=1.44=1.5B_{D(T=1S)}$	$S_1=1.44$

H.P.Gs are designed based on EBF's link beam and V.P.G's standards based on plastic shear capacity of stiff shear walls and plastic moment capacity of SMRF's columns according to AISC-Seismic Provision2010. Side columns are designed based on special moment frame's columns.

Table 2 Introduction of models

MODELS#	ABBREVIATION of MODELS
1	finite element simulation of the TRF specimen with gravity load
2	Test
3	Verification of the test by finite element simulation (Shell Element)
4*	V.P.G with non-compact web ($t_w=0.3$ mm)
5*	Simple base joint of the side columns
6*	Decreasing clear distance of H.P.Gs' web stiffeners
7*	Decreasing clear distance of H.P.Gs' web stiffeners & V.P.G with non-compact web
8*	Increasing clear distance of V.P.G's web stiffeners & decreasing them for H.P.Gs
9*	Replacing the section of side columns with IPB120 & decreasing clear distance of H.P.Gs' web stiffeners

*Models 4-9 are similar to model 3 having differences indicated in the above table.

Table 3 Geometric properties of TRF members

<i>e</i> (H.P.Gs' Length)=0.55 m , Story Height: 1.5 m, MODELS#:1-3, 5, 6, 8		
Side Columns	V.P.G (cm)	H.P.Gs (cm)
IPB100 (MODEL9 IPB120)	$t_f=1$	$t_f=1$
	$b_f=10$	$b_f=7$
	$t_w=0.4$	$t_w=0.3$
	$h_w=26$	$h_w=13$

t_f : flange thickness, b_f : flange width, t_w : web thickness, h_w : web height.

Table 4 Clear distance and dimensions of web stiffeners and continuity plates

MODELS#	Side Columns (cm)	V.P.G (cm)	H.P.Gs (cm)
1-5	$t_s=2$	$t_s=1$	$t_s=1$
		$h_s=24$	$h_s=13$
		$b_s=4.5$	$b_s=3.3$
		$a=30$	$a=12.3$
6,7&9	$t_s=2$	$t_s=1$	$t_s=1$
		$h_s=24$	$h_s=13$
		$b_s=4.5$	$b_s=3.3$
		$a=30$	$a=10.5$
8	$t_s=2$	$t_s=1$	$t_s=1$
		$h_s=24$	$h_s=13$
		$b_s=4.5$	$b_s=3.3$
		$a=75$	$a=10.5$

t_s : stiffeners thickness, h_s : stiffeners height, b_s : stiffeners width, a : clear distance of web stiffeners.

Proportion of width to thickness is considered highly ductile members. Members and web stiffeners of models which are introduced in Table 2 are shown in Table 3 and Table 4, respectively. V.P.G's height to side columns' height ratio is taken as 2.6.

As observed in the results of the analysis of TRF system, gravity load in V.P.G is less than the side columns because of the short length of H.P.Gs and existence of three vertical members in TRF system. Therefore, V.P.G as a lateral resistant and ductile member has no global buckling and brittle fracture due to axial load. Besides, V.P.G can be designed with no gravity load applying to it by placing steel deck in a proper direction. To make sure that panel zones will not yield, additional plates with 1 cm and 0.6 cm thickness are added to the side columns and V.P.G.

4.2 Experiment instance and test setup

Fifty tons capacity static hydraulic jacks and load cells which are installed at two sides of frame as shown in the Fig. 5(a) are used to apply and measure force. Three Linear Variable Displacement Transducers (LVDTs) (500 mm) are installed to measure lateral displacement. Three LVDTs (100 mm) are set to measure out of plane deformations and six 25 mm diagonal LVDTs are installed to survey diagonal deformation and chord rotation caused by shear yielding and the rest of LVDTs

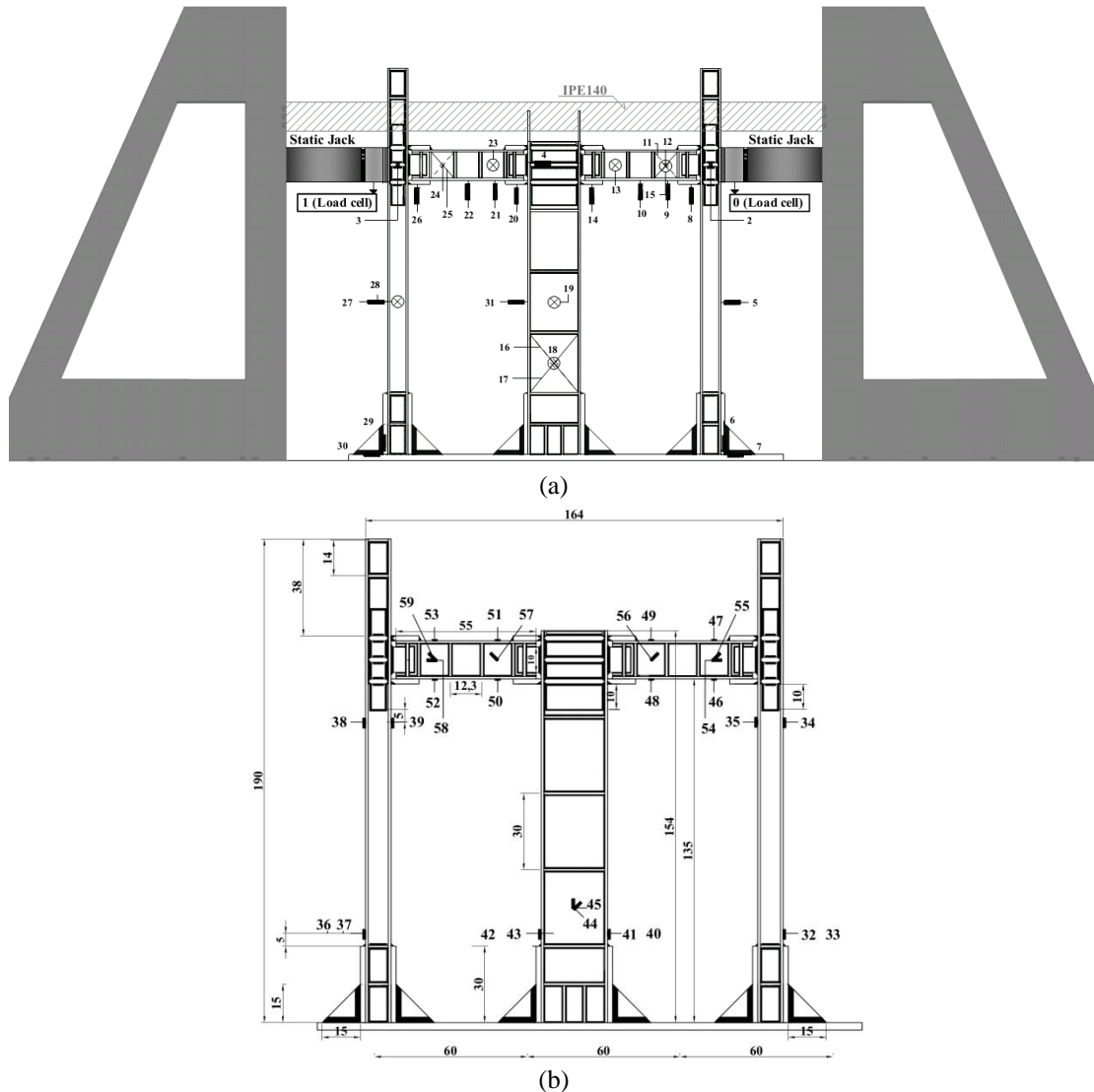


Fig. 5 Test setup: (a) load cells (0-1#), LVDTs (2-31#), and etc, (b) strain gauges (32-59#)

control accuracy of experiment. Out of plane torsion and buckling is controlled by two adjacent IPE140 placed at the top of frame in Fig. 5(a) (Farshchi *et al.* 2011). Moreover, twenty eight 5 mm strain gauges of 120 Ω (2% strains, gauge factor 2.23) are installed on the frame. These are installed in the most probable yield places to monitor specifically shear yielding along 135 and 45 angles on the web in Fig. 5(b). In order to help observe the yielding patterns and progression, steel specimens are whitewashed by lime in the test center.

4.3 Finite element models

Non-linear behavior in ABAQUS are studied by von Mises stress in accordance with yield

Table 5 Results of tensile test of plates used in the experiment and numerical models

Plates Thickness (mm)	Yield stress F_y (kg/cm ²)	Ultimate stress F_u (kg/cm ²)	Ultimate strain ϵ_u	Plastic strain ϵ_p
3	2636.85	4609.15	0.236	0.2339
4	2701.35	4360.51	0.256	0.254
6	2649	4745.44	0.22	0.2165
10	2497	4461.3	0.25	0.246
20	2534.9	5127	0.177	0.1745

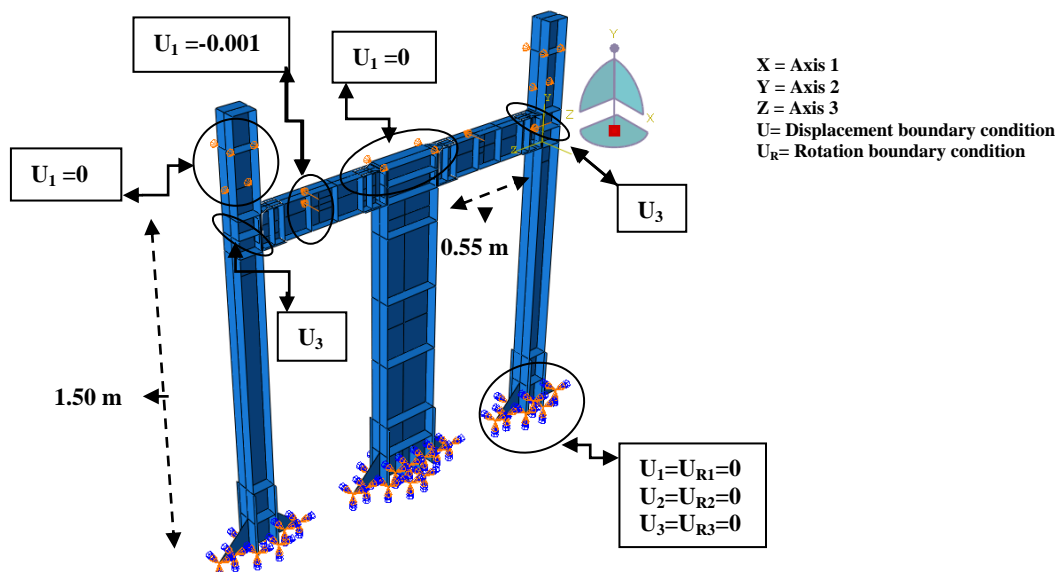


Fig. 6 Boundary conditions

stress (Bahrampoor and Sabouri 2010) and shear stress (S_{12}) in order to ensure that, members will yield at $\frac{F_y}{\sqrt{3}}$. Reduced integration shell element (S4R) is applied for defining elements to study the strain caused by transverse shear force. H.P.Gs, angles and web stiffeners are merged together at mesh's knot points. V.P.G and side columns with continuity plates, web stiffeners, and etc are merged at knot points of mesh. H.P.Gs' flanges and bearing plates are only tied wherever their surfaces are close to each other in order to make the degrees of freedom equal in this pair of surfaces. Web angle's leg and vertical members' flanges are also tied together only where the surfaces are close to one another. Approximate size for each mesh of H.P.Gs and their merged parts are defined as $1 \times 1 \text{ cm}^2$. Also, they are defined as $2 \times 2 \text{ cm}^2$ for side columns, V.P.G and other members. Static general analysis and non-linear kinematic hardening are used with consideration of non-linear geometry. In the Table 5, behavioral parameters of material are derived by standard experiment ASTM-E8-04. Members' boundary conditions are defined as shown in Fig. 6.

5. Non-linear assessments and analyses

5.1 Experiment

According to the approximate equality (ultra low relative difference (2.7%)) in the values of forces and residual deformations of the test specimen under cyclic loading observed by numerical study, there was no need to apply any gravitational load for test.

At the cycle 6 of main protocol began, uniform yield in whole panels of H.P.Gs, development of cracks in the whitewashed paint and detaching from steel plates happened all over the webs. All these phenomena were proved by high values of strain recorded by diagonal strain gauges. At the end of cycle 17 and the beginning of cycle 18, system's non-linear behavior occurred right at lateral displacement of 7.6 mm, by development of H.P.Gs' web plastic deformation and formation of diagonal tension field. In addition, at the end of cycle 17 because of the force redistribution, yield of V.P.G's web occurred. Phenomena such as formation of diagonal tension field along tensions' main directions, plastic chord rotation, local cracks in the whitewashed paint of H.P.Gs' flanges and stiffeners, and out of plane deformation of H.P.Gs' web that is called wrinkling, occurred during the experiment because of H.P.Gs' shear yielding. At the 30th cycle, next mechanism reached its critical limit as permanent deformations were increased. After this cycle, diagonal deformation and wrinkling of H.P.Gs' web were the main phenomena that determine capacity of system (Fig. 7(a)). Axial strain gauges located at H.P.Gs' web indicated that no axial force was being applied. Hence, buckling in link beams (H.P.Gs) was avoided and it is one of the important advantages of TRF. There was also a diagonal tension field formed in V.P.G's panels right at cycle 30, especially near base joint (Fig. 7(b)).

At the beginning of 33rd cycle, load was transferred to the V.P.G as a stiffened member, as a result of plastic out of plane deformation and wrinkling at the H.P.Gs' web without any significant loss of resistance. In addition, shear mechanism and formation of plastic hinges resulted in a loss of capacity. Maximum lateral displacement was 51.15 mm at 33rd cycle (Fig. 8(a)). As it is shown in Fig. 8(a), yield has been occurred in the whole length of H.P.Gs' and V.P.G's webs because of

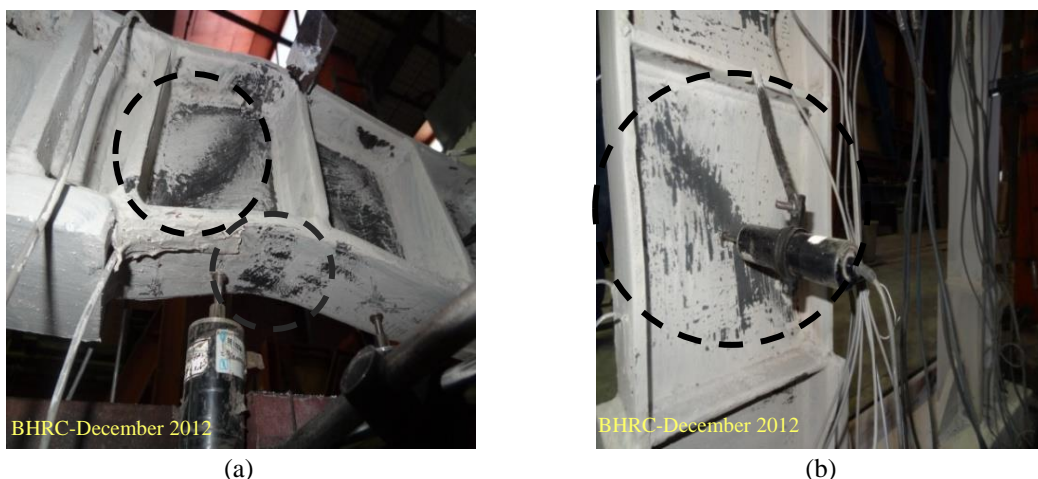


Fig. 7 Uniform shear yielding and diagonal tension field (30th cycle) formation in web of: (a) H.P.G, (b) V.P.G



(a)



(b)

Fig. 8 TRF frame deformations at the last cycles: (a) Before applying the backward load of last cycle of experiment (33rd), (b) at the end of 33rd cycle and applied forward load at 34th cycle as 57 mm lateral displacement

appearing cracks in the whitewashed paint and their plastic chord rotation. Therefore, shear yielding of ductile members of TRF before side columns is proved. Rupture of H.P.Gs' web and plastic hinge formation in vertical members near joint and panel zone at the 34th cycle is shown in Fig. 8(b). Such large deformations and resultant failure indicates that the test's end point should be considered at the previous cycle (33rd cycle). Yielding mechanism sequence for evaluation of TRF was: 1. Uniform shear yielding in H.P.Gs' web; 2. Out of plane deformation as wrinkling and diagonal tension field formation in H.P.Gs' web; 3. Local yield of H.P.Gs' flanges around the web stiffeners by formation of diagonal tension field (Fig. 7(a)); 4. Shear yielding and then formation of diagonal tension field in V.P.G's web; 5. H.P.Gs' web crippling due to shear buckling and buckle of its compression flange in web; 6. Plastic hinges formation in vertical members. Hysteresis curve of experimental model is illustrated in Fig. 9.

Fig. 9 shows a stable hysteretic behavior with adequate energy dissipation caused by plastic deformation without any loss of lateral resistance and stiffness up to capacity limit. Besides, the

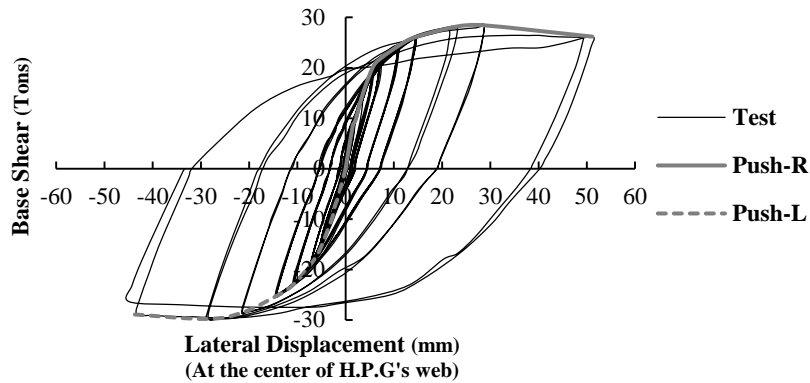


Fig. 9 Hysteresis curve of model 2 (experiment) and its push curves in each cycle

Table 6 Chord displacement surveyed by LVDTs and amount of shear deformation, in the last panel of link beams (H.P.Gs)

Lateral Displacement (mm)	LVDT#	δ_{Ch} (mm)	δ_V (mm)	LVDT#	δ_{Ch} (mm)	δ_V (mm)
10.93	11	1.38	1.95	24	0.55	5.74
-10.88	12	1.49	2.11	25	0.698	1
28.75	11	6.5	9.19	24	2.574	3.65
49.25	9	-	20	22	-	15
-43.3	9	-	22	22	-	17

figure indicates suitable design of web stiffeners. Gradual degradation of resistance and deterioration of stiffness is one of the advantages of this system.

Amount of shear displacement corresponding to diagonal LVDT in the last panel of H.P.G is calculated and listed in Table 6.

By using geometrical relations and Eqs. (4)-(6) and (7), H.P.Gs' yield and capacity limit for chord rotation will be calculated as:

$$\gamma_y = \arctan\left(\frac{1.7}{550}\right) = 0.00309 \text{ rad}, \gamma_p = \arctan\left(\frac{20}{248}\right) = 0.08 \text{ rad};$$

$$K_{eq} = 37940 \text{ Kg.cm}^{-1}, Q_{CE} = V_p = 5920.2 \text{ Kg}, \gamma_y = \frac{5920.2}{55 \cdot 37940} = 0.00283 \text{ rad};$$

Calculations show complete match between theoretical and real amounts of chord rotation. Relative rotational displacement of story $\left(\left(\frac{51.15}{1425}\right) = 0.0358 \text{ rad}\right)$ in comparison to H.P.Gs' rotation capacity limit is a sign of high plastic rotation capacity and economical and optimum design of joints with proper lateral stiffness.

5.2 Finite element analyses

5.2.1 Verification and seismic characteristics

Verification of the developed numerical studies by finite element simulation is carried out by analyzing the shear yielding through presentation of von Mises stresses and transverse shear

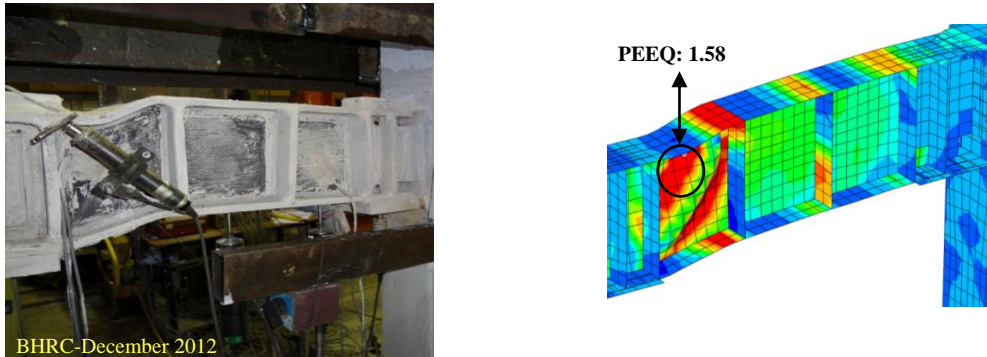


Fig. 10 Yield and deformation of H.P.G in TRF specimen and its finite element model

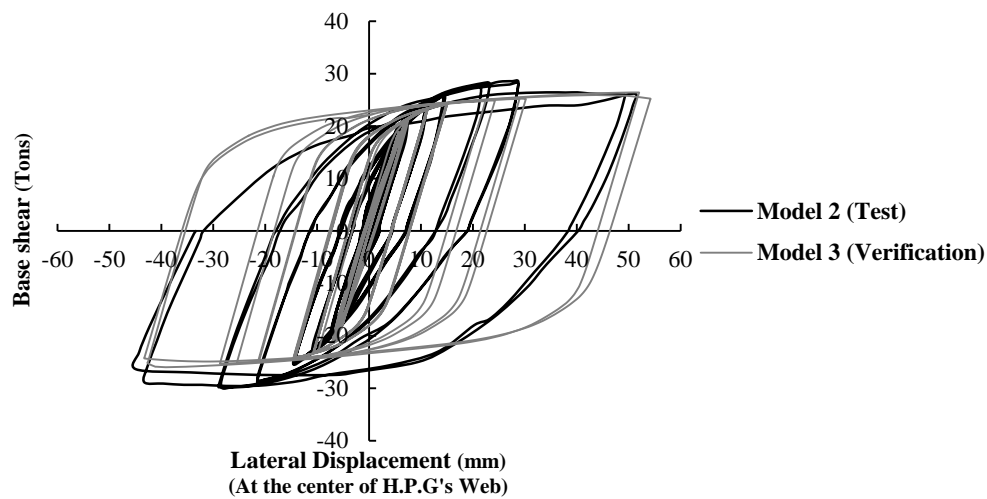


Fig. 11 Verification of hysteresis curves of model 2 and model 3

Table 7 Seismic characteristics of TRF specimen and its finite element model

MODELS#	Δ_y (mm)	Δ_{max} (mm)	μ	
2	7.6	51.15	6.73	
3	6.98	51.17	7.33	
Relative Difference (%)	8.2	-	8.18	
MODELS#	V_y (kg)	K_e^* (Kg/mm)	V_{max} (kg)	
2	22168	2916.84	-29801	28560
3	23294.9	3337.51	-25729	26408.2
Relative Difference (%)	4.8	12.6	11.36	7.5

*Effective stiffness, corresponding to slope of first line of bilinear capacity diagram, elastic stiffness.

tension as S_{12} .

Plastic equivalent strain (PEEQ) as a scalar measure of the accumulated plastic strain of H.P.Gs' web in model 3 at 33rd cycle is illustrated in Fig. 10. This parameter equals to 1.58,

simulating the rupture of members and defining when the analyses end. In Fig. 10 according to von Mises stresses, web diagonal yield due to diagonal tension field action, shear buckling, and wrinkling phenomena are illustrated. Also, the members' web doesn't have any sign of elastic buckling; therefore, stability design is approved. Hysteresis curve and seismic characteristics are illustrated in Fig. 11 and Table 7 (V_y , V_{max} : Yield and Maximum Base Shear) which approve system's high ductility in addition to sufficient lateral stiffness.

In addition, residual deformations with relative difference of 12.5 %, between experiment and finite element model prove the accuracy of simulation. Since, there is no sudden decrease in experiment's hysteresis curve; it is shown that stiffeners are placed at proper distances to control local buckling.

Energy dissipation by plastic shear deformation in all loading cycles is obtained 1.76×10^6 Kg.cm by finite element model and 1.46×10^6 Kg.cm by experiment which are the area of hysteresis loops in Fig. 11. Thus, verification with relative difference of 17.1 % is proved.

Amount of shear deformation of V.P.G's panel can be calculated during the test by LVDT 16,

Table 8 Chord and shear deformation of model 2 and 3, in the last panel of V.P.G

Load	MODELS#	LVDT#	$\delta_{Ch,y}$ (mm)	$\delta_{V,y}$ (mm)	$\delta_{Ch,Max}$ (mm)	$\delta_{V,Max}$ (mm)
Forward Load	2	16	1.14	1.61	10.44	14.75
	3	16	-	1.6	-	15
Relative Difference (%)			-	0.6	-	1.7
Forward Load	2	17	1.54	2.02	11.11	15.7
	3	17	-	1.83	-	15.3
Relative Difference (%)			-	9.4	-	2.55
Backward Load	2	16	1.44	2.03	9.94	14.05
	3	16	-	1.81	-	15.1
Relative Difference (%)			-	10.8	-	7.5
Backward Load	2	17	1.52	2.15	11.8	16.68
	3	17	-	1.9	-	15.29
Relative Difference (%)			-	11.6	-	8.33

Table 9 Values of strains in model 2 and 3, in the flanges of V.P.G and H.P.Gs

		Strain gauges#											
		40	41	42	43	46	47	48	49	50	51	51	53
		Strains $\times 10^{-3}$											
Y.P	M 2	1.28	1.44	1.04	1.18	0.197	0.194	1.42	0.183	0.75	0.84	0.198	0.196
	M 3	1.21	1.28	0.96	1.06	0.182	0.18	1.31	0.18	0.73	0.8	0.18	0.181
R.D (%)		5.79	12.5	8.33	11.3	8.24	7.78	8.4	1.67	2.74	5	10	8.29
U.P	M 2	13.1	14.1	12.3	12.6	14.7	14.1	2.26	1.82	1.74	1.81	14.2	14.6
	M 3	12.3	13.2	11.8	12.1	13.4	13.2	2.07	1.7	1.6	1.7	13.1	13.05
R.D (%)		7.01	6.57	4.41	4.06	10.17	6.89	9.18	7.06	8.75	6.47	8.4	11.8

M 2: Model 2, M 3: Model 3, Y.P: Yield Point (cycle 18), U.P: Ultimate Point (cycle 33), R.D: Relative Difference.

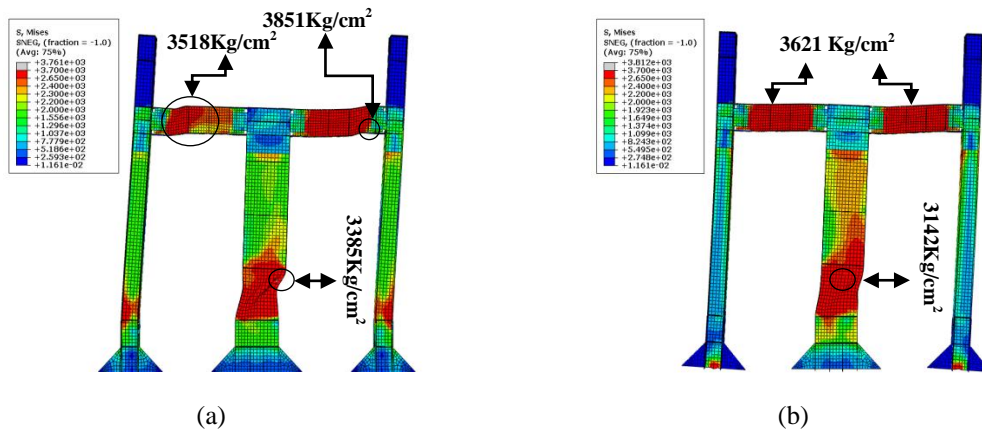


Fig. 12 von Mises stresses in: (a) model 4, (b) model 5

LVDT 17 and using the Eq. (10). Then, it will be compared with the same parameters in finite element model (Table 8). As a result, Table 8 shows complete match between the amount of V.P.G’s shear deformation in model 2 and model 3, that proves the accuracy of the verification ($\delta_{Ch, y}$, $\delta_{Ch, Max}$: Yield and Maximum Chord Deformation and $\delta_{V, y}$, $\delta_{V, Max}$: Yield and Maximum Shear Deformation).

According to Table 9, the accuracy of the verification is validated by the approximate equality in the values of strains that are monitored by the strain gauges (which are installed on the flanges of V.P.G and H.P.Gs) and the finite element model.

5.2.2 Numerical studies

In model 4, the thickness of V.P.G’s web is changed to 3 mm, while other geometric properties are the same as model 3. von Mises stresses of model 4 illustrates that reducing web thickness of V.P.G results in a reduction of strength capacity of TRF due to out of plane deformation of V.P.G’s web which is a result of shear yielding (Fig. 12(a)). In this model, simultaneous yielding happens in V.P.G and H.P.Gs. Also, out of plane deformation caused by tension field action of ending panel of V.P.G’s web requires attention to stiffeners emplacement. Fig. 12(b) shows von Mises stresses in model 5 having side columns with simple base joints. Also, ductile behavior of TRF is proved by widespread shear yielding of V.P.G’s web panels in comparison to model 3.

In subject of gaining stability by placing web stiffeners according to Eq. (2) in model 6, von Mises stresses, and deformations of this model in Fig. 13(a) illustrates that without any significant increase of stiffness, shear buckling can be controlled and ductility factor is improved.

According to von Mises stresses of model 7 (V.P.G with non-compact web) as shown in Fig. 13(b), shear capacity is decreased by out of plane deformation caused by shear yielding in V.P.G’s web, redistribution of force to the side columns, and plastic hinges formation.

In the model 8 distance of V.P.G’s web stiffeners according to Eq. (3) are increased to the clear distance of web stiffeners used to develop the web shear strength (a_{oi}). As it is shown in Fig. 14(a) ductility is limited by shear buckling and plastic hinges formation in vertical members. Effect of side columns’ stiffness on TRF behavior is shown in model 9 by replacing the section with IPB120. This results in an increase of capacity and leads to better seismic characteristics, while shear yielding is progressing in H.P.Gs due to deformation and von Mises stresses (Fig. 14(b)).

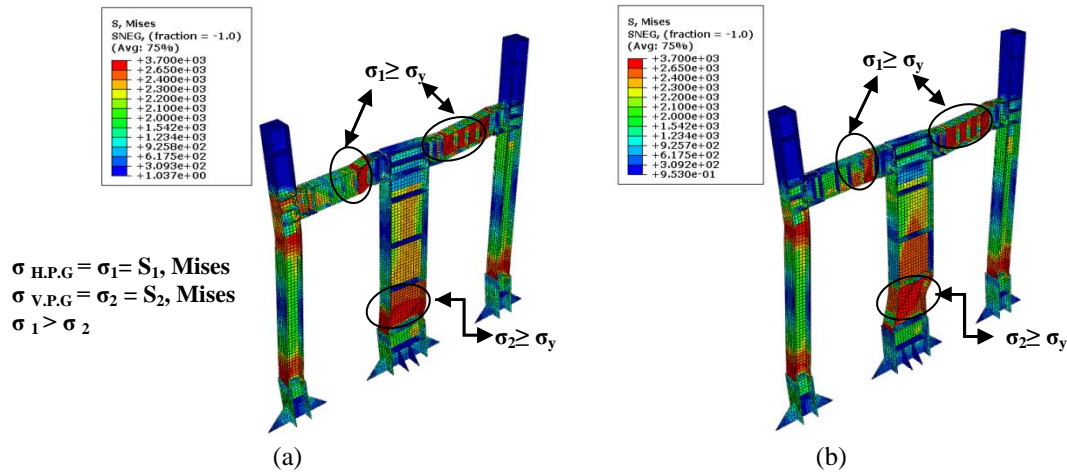


Fig. 13 von Mises stresses in: (a) model 6, (b) model 7

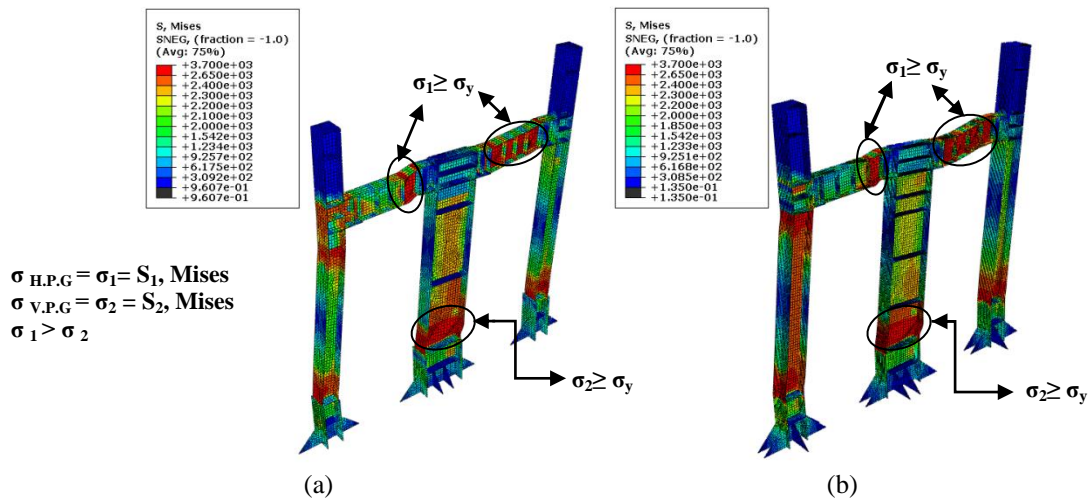


Fig. 14 von Mises stresses in: (a) model 8, (b) model 9

5.2.3 Comparison of seismic characteristics

Seismic characteristics of the models are indicated in Table 10. In the model 4 by reducing V.P.G's web thickness lateral resistance and stiffness decrease due to reduction of plastic shear capacity of V.P.G whereas, ductility factor is the same as model 3.

In the model 5, appropriate lateral stiffness with decrease of base shear capacity are assessed because of its simple base joint of side columns and the same ductility in comparison to model 3.

By decreasing the clear distance of H.P.Gs' web stiffeners in model 6, maximum lateral displacement is increased without any significant rising of lateral stiffness and resistance (Table 10). Highest ductility factor as it is shown Table 10, belongs to model 6 which has decreased the number of H.P.Gs' web stiffeners to prevent shear buckling and wrinkling. Small percentages of strain hardening in Table 10, is achieved in models 4 and 6, due to its high plastic deformations and ductile behavior. In model 7, according to Table 10, lateral resistance and stiffness are

Table 10 Seismic characteristics of models 2, 3-9

MODELS#	Δ_y (mm)	Δ_{max} (mm)	μ	
2	7.6	51.15	6.73	
3	6.98	51.17	7.33	
4	6.57	51.22	7.8	
5	6.94	50.9	7.33	
6	7.28	59.92	8.24	
7	6.74	45.99	6.82	
8	6.8	41.1	6.04	
9	7.69	54.35	7.06	
Shear Yielding of Link Beams (H.P.Gs) Rigid Base Join of Side Columns $\mu=7.2$		Shear Yielding of Link Beams(H.P.Gs) Simple Base Join of Side Columns $\mu=7.33$		
MODELS#	V_y (kg)	K_e (Kg/mm)	V_{max} (kg)	Strain hardening (%)
2	22168	2916.84	28560	-
3	23294.9	3337.51	26408.2	2.11
4	20573.5	3132.63	21245.3	0.48
5	14899	2146.51	15795.9	0.95
6	24251.07	3332.85	25232.12	0.56
7	21347.2	3165.6	22611.67	1.02
8	23549.6	3315.5	25979.2	1.88
9	32197.66	4183.65	35493.3	1.69

decreased due to reduction of V.P.G's web thickness and its plastic shear capacity.

According to Table 10, in the model 8 by increasing the clear distance of V.P.G's stiffeners, least ductility factor is achieved due to local buckling and out of plane deformation of V.P.G's web. By increasing side columns' strength in the model 9, maximum base shear capacity of TRF due to transferring force to them, is obtained (Table 10).

Comparison between TRF and passive control by vertical link beam in EBF system proves that TRF has better lateral behavior because of yield in three ductile members and lateral stability derived from members' shear stiffness. In the experiment, TRF had ductility factor of 6.7 and lateral stiffness of 2916.8 kg/mm. Therefore, TRF presents higher ductility and stiffness in comparison to EBF with vertical link beam that was investigated by Zahrae (2009) having corresponding amounts of 4.3 and 2734.5 kg/mm.

6. Conclusions

The objective of this paper is to introduce TRF as a ductile and lateral resistant system in its hysteretic behavior. Besides, it offers a design method for H.P.Gs and V.P.G considering their shear yielding based on experimental and numerical studies. Following are primary conclusions achieved:

- Ductility factor of TRF with shear yielding of link beams (H.P.Gs) is estimated 6.7 with

lateral stiffness of 2916.8 kg/mm from experiment and these parameters are evaluated by finite element models as 7.3 and 2146.5 kg/mm for its finite element model having simple base joint of side columns. This illustrates that TRF has high ductility in addition to the large lateral stiffness simultaneously.

- Proper behavior of TRF system during shear yielding of its H.P.Gs' web results in: 1. Increasing plastic chord rotation capacity; 2. Controlling connection rotation and relative rotation of stories; 3. Using entire capacity of web along the beams; 4. Conformance to weak beam and strong column requirements.

- Stable, progressive and voluminous hysteresis curve without any significant lateral resistance degradation and deterioration of stiffness (up to capacity limit), is assessed from experiment.

- TRF with simple base joint of side columns and its V.P.G behaves like a ductile lateral resistant system with more lateral stiffness compared to Eccentrically Braced Frame without axial force in its link beams. Additionally, presence of two link beams (H.P.Gs) in spite of one in EBF, results in higher degrees of indeterminacy in comparison to EBF.

- Different seismic characteristics sensitivity to any change of resistance properties is observed especially width to thickness ratio in the web of H.P.Gs and V.P.G. It is concluded that width to thickness ratio is better to be like high ductile members.

- If clear distance between V.P.G's web stiffeners is considered less than $a = \frac{(50 \cdot t_w - \frac{d}{5}) + a_{oi}}{2}$, ductility factor will be increased by controlling shear buckling in V.P.G's web.

- Rigid connections of TRF's link beams (H.P.Gs) with shear yielding of its H.P.Gs will be optimal by designing in accordance with section expected moment capacity as $M_{CE} = \frac{V_P \cdot e}{2}$ that is smaller than section plastic moment capacity (M_P).

Acknowledgements

The experiment was conducted in structure laboratory of Building and Housing Research Center in Iran (BHRC). Hereby, we appreciate all their technical assistance. Though, all rights of this research and its results are reserved by authors of this paper.

References

- Ashtari, P. and Abbasi, A.A. (2010), "Evaluation of response modification factor of different shape of TBR", *International Conference on Seismology*, Kerman University, Kerman, Iran.
- Ashtari, P. and Bandehzadeh, M. (2009), "Seismic evaluation of new crucial beam-column lateral resistant system", *8th National Congress on Civil Engineering*, Shiraz University, Shiraz, Iran.
- Ashtari, P., Hamed, F., Barzegar Sedigh, H. and Rasouli, I. (2012), "Comparison of seismic responses of T Resistant Frame (TRF) with shear or bending yielding in link beams", *15th World Conference on Earthquake Engineering*, Lisbon, Portugal.
- Bahrampoor, H. and Sabouri Ghomi, S. (2010), "Affect of easy-going steel concept on the behavior of diagonal eccentrically braced frames", *J. Civil Eng.*, **8**(3), 242-255.
- Bandehzadeh, M. and Ashtari, P. (2014), "T-Resisting Frame concept: headway towards seismic

- performance improvement of steel frames”, *J. Constr. Steel Res.*, **104**, 193-205.
- Barzegar Sedigh, H. (2013), “Investigation of seismic behavior of T Resistant Frame (TRF) with link beams having shear or moment yielding”, Thesis for the degree of Master of Science, Department of Civil Engineering, Faculty of Engineering and Technology, Imam Khomeini International University, Qazvin, Iran.
- Chao, Sh. and Goel, S.C. (2005), “Performance based seismic design of EBF using target drift and yield mechanism as performance criterion”, A Report on Research, Department of Civil & Environment Engineering, University of Michigan, USA.
- Farshchi, H., Moghadam, A.S. and Jazany, R.A. (2011), “Experimental and analytical study of connection strength effect in X-type braced frames”, *Modares J. Civil Eng.*, **11**(4), 69-134.
- FEMA 274 (1997), Federal Emergency Management Agency, NEHRP Commentary on guidelines for the Seismic Rehabilitation of Buildings, Report No 274, Washington DC, IL.
- FEMA 356 (2000), Federal Emergency Management Agency, NEHRP Guidelines for the Seismic Rehabilitation of Buildings, Report No 356, Washington DC, IL.
- Gorzin, M. (2011), “Seismic assessment of TBF resistant frame with endurance time method”, Thesis for the degree of Master of Science, Civil Engineering Department, Faculty of Engineering, Zanjan University, Zanjan, Iran.
- Hajnajafi, L. and Tehranizadeh, M. (2013), “Evaluation of seismic behavior for moment frames and eccentrically braced frames due to near-field ground motions”, *Asian J. Civil Eng. (BHRC)*, **14**(6), 809-830.
- Krawinkler, H. (2009), “Loading history for cyclic testing in support of performance assessment of structural component”, Department of Civil and Environment Engineering, Stanford University, Stanford, California, USA.
- Lignose, D. and Krawinkler, H. (2008), “Side way collapse of deteriorating structural system under seismic excitations”, Thesis for the degree of Doctor of Philosophy, Stanford University, Stanford, California, USA.
- Riahi, H.T. and Estekanchi, H.E. (2010), “Seismic assessment of steel frames with the endurance time method”, *J. Constr. Steel Res.*, **66**(6), 780-792.
- Sabouri, G.S. (2001), *Lateral Resistant Systems, Introduction of Shear Walls*, Angizeh Publication, Tehran, Iran.
- Zahrae, S.M. (2009), *Behavior of Vertical Link Beam in Steel Building*, BHRC Publish No. R-515, Tehran, Iran.
- AISC341-10 (2010), Seismic Provisions for Structural Steel Buildings, ANSI-AISC 341-10, American Institute of Steel Construction, Chicago, IL.
- ASCE/SEI 7-10 (2010), Seismic rehabilitation of existing buildings, s.l., American Society of Civil Engineers, IL.